nature photonics

ARTICLES

https://doi.org/10.1038/s41566-021-00814-x

Multistep staircase avalanche photodiodes with extremely low noise and deterministic amplification

Stephen D. March[1]✉, Andrew H. Jones[2], Joe C. Campbell[2] and Seth R. Bank[1]✉

In 1982, Capasso and co-workers proposed the solid-state analogue of the photomultiplier tube, termed the staircase avalanche photodiode. Through a combination of compositional grading and small applied bias, the conduction band profile is arranged into a series of steps that function similar to the dynodes of a photomultiplier tube, with twofold gain arising at each step via impact ionization. A single-step staircase was previously reported but did not demonstrate gain scaling through cascading multiple steps or report noise properties. Here we demonstrate gain scaling of up to three steps; measurements show the expected 2^N scaling with the number of staircase steps, N. Furthermore, measured noise increased more slowly with gain than for photomultiplier tubes, probably due to the lower stochasticity of impact ionization across well-designed heterojunctions as compared with the secondary electron emission from metals. Excellent agreement was found between the experiments and Monte Carlo simulations for both gain and noise.

Photomultiplier tubes (PMTs) are often regarded as the preferred family of detectors for ultraviolet to near-infrared applications, due to their extremely high signal gains (>10^6) and superior low-noise performance[1]. In the decades since the first reported PMT[2], these characteristics enabled seminal fundamental scientific breakthroughs such as single-photon counting[3,4], and advances in radioimmunoassay[5], positron emission tomography[6], high-energy physics[7,8], X-ray astronomy[9] and electron microscopy[10]. Photomultiplier tubes continue to facilitate advances in biomedicine using superresolution[11] and multiphoton[12] microscopy, as well as numerous other industrial applications[13]; they rely on large potential differences between adjacent metallic dynodes to produce a cascade of secondary electrons, as illustrated in Fig. 1a. Secondary electron emission per dynode stage obeys Poissonian statistics, with yields varying from ~1–4[14–16]. Variation in the output gain (M) for detectors is typically parameterized by the excess noise factor, $F(M) \equiv \langle M^2 \rangle / \langle M \rangle^2 \geq 1$, where a value of unity indicates noiseless amplification.

Despite their advantages, PMTs suffer from high operating voltages (>1 kV), large sizes (~1 to 10 cm), sensitivity to mechanical and magnetic perturbations, fragile vacuum tubes and high production costs[1]. Conventional avalanche photodiodes (APDs) are an attractive solid-state alternative as they can leverage semiconductor integration to produce arrays, require lower operating voltages (<100 V), possess more compact and rugged form-factors and typically offer lower costs[17]. Conventional APDs are designed with a high-field depletion region that produces multiplication gain via impact ionization; however, gain variations arise from the stochastic nature of impact ionization, which is exacerbated when both electrons and holes are capable of initiating impact ionization events. It is well-established in the APD community that single-carrier-initiated impact ionization[18] and discrete localization of impact ionization events[19,20] are required for the lowest noise APD performance.

Strategic heterojunction placement in APD structures can meet both requirements, as they simultaneously propel charge carriers above the impact ionization energy threshold when crossing heterointerfaces and provide charge carriers with further energy due to band discontinuities, resulting in a change in the relative optical phonon scattering rate between electrons and holes[21]. In particular, Capasso and colleagues[22,23] proposed a staircase APD structure that incorporates graded bandgaps across heterojunction interfaces. The staircase design, shown in Fig. 1b, offers a paradigm shift for low-noise device operation by localizing impact ionization at discrete regions of the structure, thus producing deterministic gain while simultaneously promoting single-carrier initiated impact ionization. It was heralded as the solid-state implementation of the PMT, where the role of PMT dynodes is replaced by the staircase steps.

The first attempted staircase APDs using the GaAs–AlGaAs material system[24,25] suffered from insufficient band offsets, and high-energy charge carriers probably experienced intervalley scattering before impact ionizing[26]. Further attempts at using GaP–AlInGaAs[27] and AlGaSb-GaInAsSb[28] did not clearly demonstrate discrete step gain. The $Al_xIn_{1-x}As_ySb_{1-y}$ material system (hereafter called AlInAsSb) grown as digital alloys[29,30] recently exhibited a widely tunable direct bandgap between 0.24 and 1.18 eV (ref. [30]) and has enabled conventional APDs with low excess noise[31], high gain-bandwidth product[32] and wavelength-flexible photoresponse[33,34]. Although a complication for conventional APD operation, the change in bandgap occurs almost entirely in the conduction band[35], suggesting that AlInAsSb is ideal for designing electron-initiated impact ionization structures[36]. Recent work using AlInAsSb to create a single-step staircase APD demonstrated an approximately twofold photogain enhancement across a wide wavelength range[37]; however, it was rightly pointed out[38] that this was not a clear observation of PMT-like behaviour as it demonstrated neither discrete gain scaling with the number of steps nor the predicted low-noise benefits[19,20]. Here we address these shortcomings by demonstrating both clear gain scaling with the staircase step count and low-noise operation.

Results

Deterministic gain, low-noise staircase APDs. In this work we demonstrate multistep AlInAsSb staircase APDs that produce

[1]University of Texas, Austin, TX, USA. [2]University of Virginia, Charlottesville, VA, USA. ✉e-mail: sdmarch@utexas.edu; sbank@utexas.edu

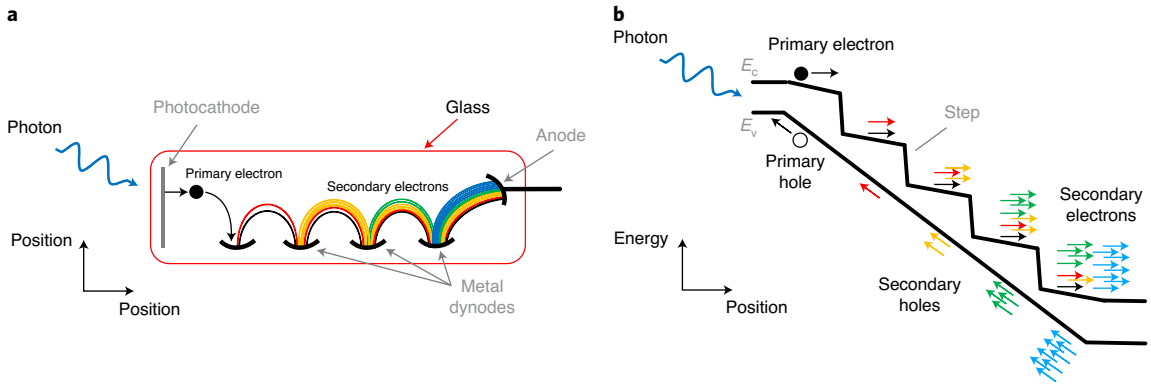

Fig. 1 | A structural comparison of a low-noise PMT and multistep staircase APD. a, A PMT with four metallic dynode stages contained within a large glass vacuum. Typical PMTs have between 6 to 13 dynodes, all separated by >100 V potentials. Primary photoelectrons generate a cascade of high-energy secondary electrons that acquire energy from the large electric fields between adjacent dynodes. The increase in the secondary electron count over the primary electron count is registered as gain in the form of photocurrent at the anode. **b**, A multistep staircase APD energy–position band diagram illustrating localized carrier multiplication at the step regions. Electron-initiated impact ionization produces secondary electrons in the conduction band (E_c) and secondary holes in the valence band (E_v). The lack of valence band discontinuity prevents hole-initiated impact ionization. Localized, single-carrier initiated impact ionization events lead to low-noise performance.

deterministic single-carrier initiated impact ionization events localized in the step regions. We show clear gain scaling, which is corroborated by Monte Carlo simulations, and find that large impact ionization step efficiency predicts low and effectively constant excess noise factors near unity. We also find that the measured staircase APD noise power scales more slowly with multiplication than early theoretical predictions and estimate the resulting signal-to-noise ratio benefit. These results advance APD development by marrying PMT-like performance with the practical advantages afforded by solid-state devices.

Design of deterministic gain multistep staircase APDs. We expand on our previous one-step work[37] by presenting one-, two- and three-step AlInAsSb staircase APD structures grown via molecular beam epitaxy (MBE). Staircase APDs were designed using an electrostatic solver to balance impact ionization in the step regions while minimizing band-to-band tunnelling dark current and carrier-trapping-enhanced gain[39]. We achieved this balance by adjusting the grade rate between the wide and narrow bandgap regions to minimize heterointerface scattering and leveraging the favourable band offsets of AlInAsSb to promote electron-only impact ionization. Figure 2a shows an example of the three-step staircase APD layer structure employed.

Impact ionization is a scattering process where both momentum and energy must be conserved. Typically, charge carriers must achieve energies that are considerably larger than the bandgap of the host material before impact ionization occurs[40]. Here we designed structures such that the electrons acquire energy that is substantially greater than the bandgap energy of the AlInAsSb at the bottom of each step. Each step simultaneously provides a large increase in electron kinetic energy while lowering the impact ionization threshold by grading into a smaller bandgap material, all on length scales comparable with the mean free path of impact ionization. Hot electrons above the impact ionization threshold impact ionize once, which doubles the photocurrent and the photogain, leading to gain that scales as 2^N, where N is the number of steps.

To assess impact ionization behaviour, we developed Monte Carlo simulations of electron and hole transport, as described in the Methods. We find in Fig. 2b–d that one-, two- and three-step staircases exhibit impact ionization events localized in the step regions that are dominated by electron initiation, making the staircase APD a spatially localized, single-carrier-initiated impact ionization device. This hints that the staircase operates under nearly ideal conditions for low-noise performance[18–20]. Simulated gain distributions are plotted in Fig. 2e and corroborate that the majority of electrons contribute to 2^N gain performance. The few electrons that do not fall in the 2^N bins probably contribute to the non-unity component of $F(M)$.

Deterministic 2^N gain scaling. To demonstrate discrete twofold gain per step, we normalized the measured photoresponse of the staircase APDs to those of otherwise-identical step-free control structures, such as the control in Fig. 2a (see Supplementary Figs. 3 and 4 for details). Monte Carlo simulations agree well with the measured data in Fig. 3a and predict similar 2^N gain performance. The average measured gains for the one-, two- and three-step structures were 1.77, 3.97 and 7.14, and the average Monte Carlo gains were 2.01, 3.81 and 6.71, respectively. We calculated the gain versus step count relationship using power law curve fits in Fig. 3b for the measured and simulated data to be 1.92^N and 1.95^N, respectively, which closely follow the ideal 2^N behaviour. Observation of deterministic 2^N gain and the aforementioned electron-initiated impact ionization (Fig. 2b–e) corroborate our expectation of single-carrier-initiated and spatially localized impact ionization events, suggesting low-noise amplification.

Impact ionization probability predicts low excess noise factors. Staircase APD step performance depends strongly on the probability, p, of impact ionization, which is fundamentally a stochastic process in the step regions. As shown in Fig. 4a, we calculated p from $\langle M\rangle = (1+p)^N$ from refs. [19,20,23] using the measured gain data for the one-, two- and three-step devices. The step probability was >0.9 for all devices, suggesting efficient and scalable impact ionization behaviour with step scaling. The link between p and $F(M)$ for staircase APDs has been previously determined using multiple independent approaches[20,23,41] and takes the form:

$$F(M) = 1 + \frac{1-p}{1+p}(1-(1+p)^{-N}) \quad (1)$$

We see from equation (1) that, as expected, the largest possible p values produce the lowest $F(M)$. Using the same fit-to-measurement p values from Fig. 4a, we calculated $F(M)$ in Fig. 4b. We found that $F(M)$ for these structures was below 1.1, suggesting that $F(M)$

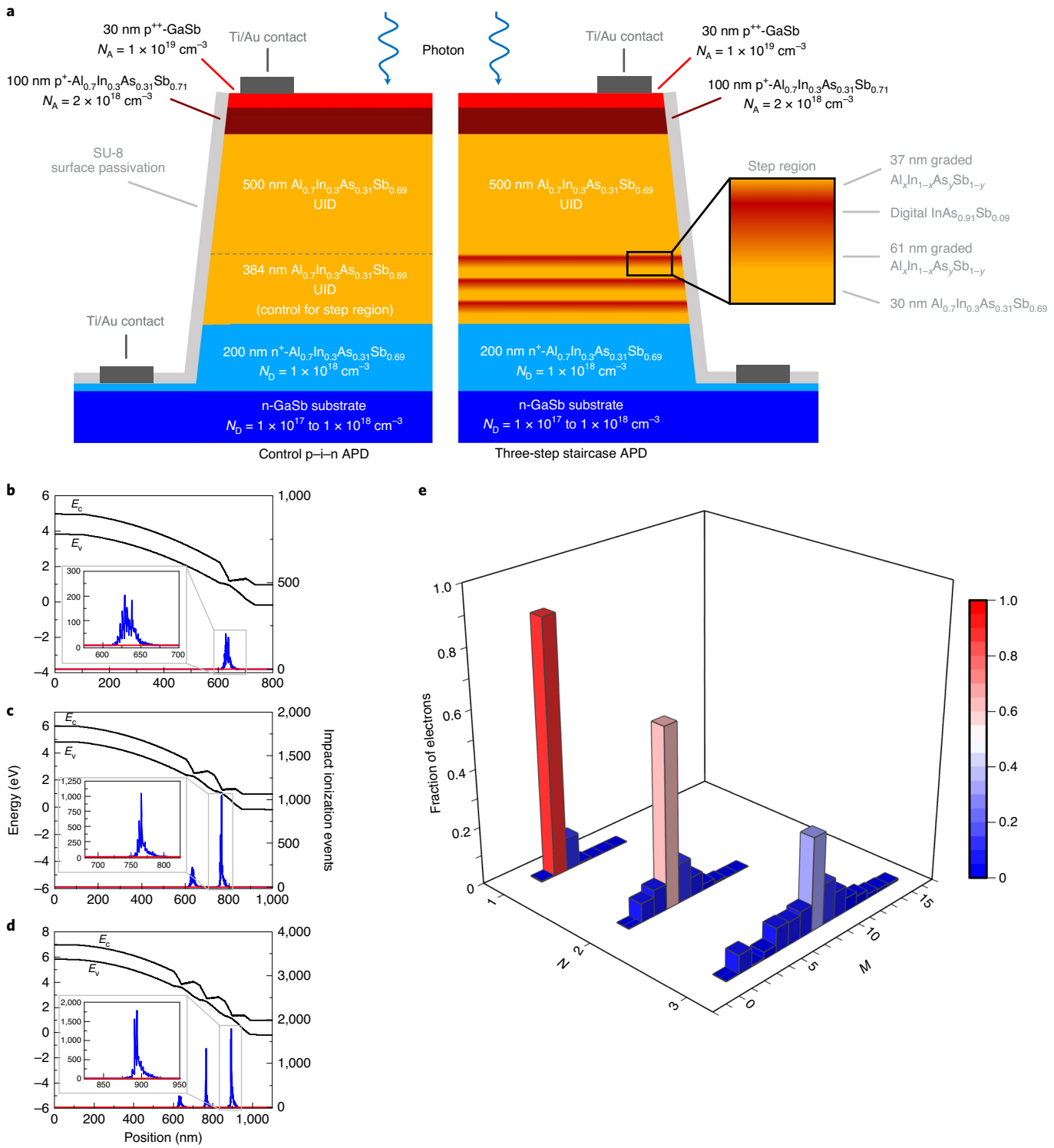

Fig. 2 | Staircase APD design used to produce localized, single-carrier 2^N gain. a, A side-by-side comparison of mesa-layer structures for a three-step AlInAsSb staircase APD (right) and its step-free control p–i–n APD (left). The step regions were composed of grading between $Al_{0.7}In_{0.3}As_{0.31}Sb_{0.69}$ and $InAs_{0.91}Sb_{0.09}$ grown as digital alloys. Moderate acceptor (N_A) and donor (N_D) doping concentrations are supplied at the top and bottom of the mesa form contact regions, as described in the Methods. In the top 600 nm of the structure, photogenerated electrons acquire energy via diffusion from the p-contact region and field drift in the ungraded $Al_{0.7}In_{0.3}AsO_{0.31}Sb_{0.69}$ unintentionally doped (UID) region; however, at sufficiently small bias values, these electrons do not reach their impact ionization threshold. Electrons that enter the step region acquire sufficient energy to initiate discrete impact ionization events, leading to low-noise behaviour. **b**–**d**, Simulated bandstructures for one- (**b**), two- (**c**) and three-step (**d**) AlInAsSb staircase APDs operating at −4, −5 and −6 V, respectively, to produce ~2^N gain. Modelled impact ionization events initiated by electrons (blue) and holes (red) indicate that electron-only initated impact ionization events dominate and are localized in the step regions. **e**, Fraction of electrons producing gain M, crossing the Nth step. The simulated gain (M) distributions of electrons for the same one-, two- and three-step staircase devices show clear spikes in the gain distributions when the gain is ~2^N.

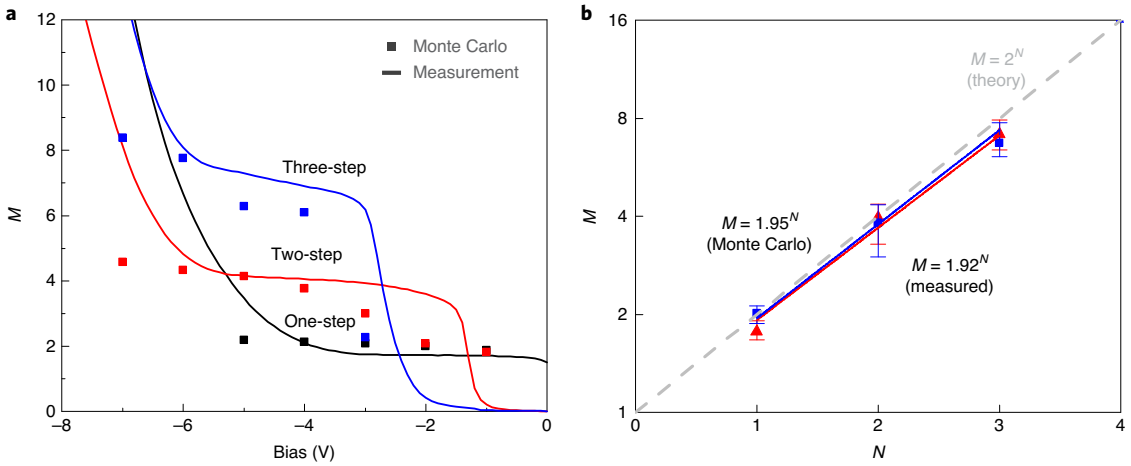

Fig. 3 | Demonstration of deterministic 2^N gain scaling. a, Measured and Monte Carlo simulated photogain for the one-, two- and three-step staircase APDs at 300 K. Measured one-step staircase data are from ref. [37]. Gain was approximately zero until a sufficient reverse bias allowed all steps in the device to reach the staircase condition, at which point the gain increased to ~2^N. The large gain increase above 2^N at higher reverse bias values indicate band-to-band tunnelling breakdown through the narrow bandgap $InAs_{0.91}Sb_{0.09}$ regions of the steps. Temperature-dependent dark current density measurements corroborate band-to-band tunnelling breakdown[48] (see the Methods and Supplementary Fig. 5). **b**, The average measured and simulated gain for one-, two- and three-step staircase APDs. Error bars indicate the range of the gain when the device was operating in the 2^N operating regime. Power law curve fits of the measured and simulated device performance closely follow 2^N theoretical performance.

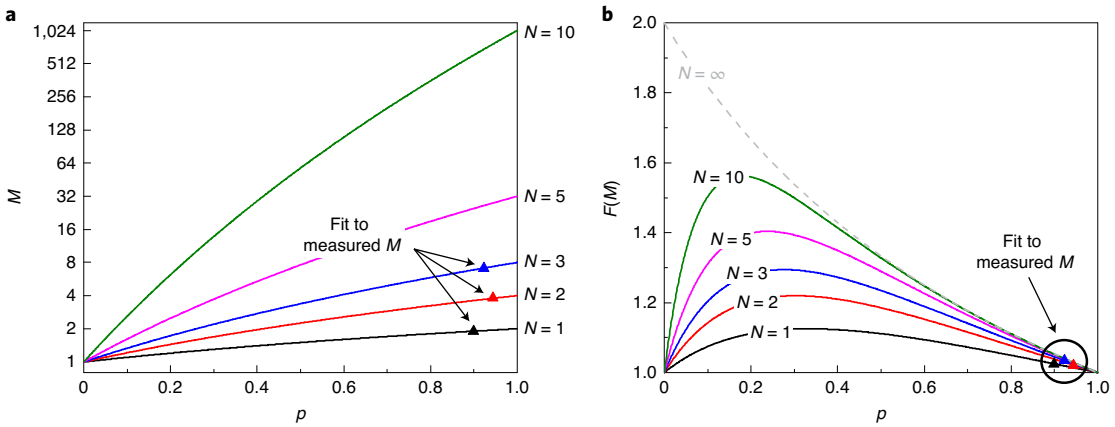

Fig. 4 | Calculated staircase APD impact ionization probability and excess noise factors. a, Impact ionization probability per step (p) calculated on the basis of average measured $\langle M\rangle$ for each staircase device found in Fig. 3. Solid lines indicate $\langle M\rangle = (1+p)^N$ for different values of N. Large p values near unity suggest stable impact ionization efficiency that scales with increased device step count. **b**, $F(M)$ calculated from fit-to-measured data of p using refs. [20,23,41]. The large p values observed suggest $F(M)$ should be low and constant with step scaling. The family of curves for $F(M)$ versus p indicate that even as N approaches infinity, $F(M)$ will remain low and approximately constant for p values near unity.

is expected to remain low and near unity as the number of steps increases; moreover, $F(M)$ should remain low even in the extreme case when the number of steps approaches infinity. Importantly, the large p values suggest staircase APDs should exhibit low shot-noise behaviour that essentially scales independently from the step count while simultaneously achieving 2^N gain scaling.

Noise comparison with other detectors. In Fig. 5a, we compare the experimentally determined $F(M)$ from Fig. 4b with Monte Carlo simulations, where $F(M)$ was calculated directly from the carrier transport using $F(M) = \langle M^2\rangle/\langle M\rangle^2$. Importantly, the simulated excess noise factors agree well with the measured data. We also compare staircase performance against the lowest expected $F(M)$ for conventional APDs (that is, when $k = 0$ in McIntrye's local field limit)[18] and one-, two-, and three-dynode PMTs (that is, when $b = 0$)[15,20]. An N-step staircase APD with extremely low and stable $F(M)$ is clearly less noisy than an N-dynode PMT and also outperforms the best case conventional APDs when the staircase operates with 2^N gain scaling.

The noise benefits of the staircase APD are not fully captured by the excess noise factor. A more useful measure of detector sensitivity is the noise power spectral density, s_f, which is typically expressed as:

$$s_f = 2q\,(I_p + I_d)\,\langle M\rangle^2 F(M)\,R + \frac{\sigma^2_{\text{circuit}}}{\Delta f} \qquad (2)$$

The first term on the right side of equation (2) is the noise associated with the detector, where q is the elementary charge, I_p and I_d are the average photo and dark currents, and R is the AC load

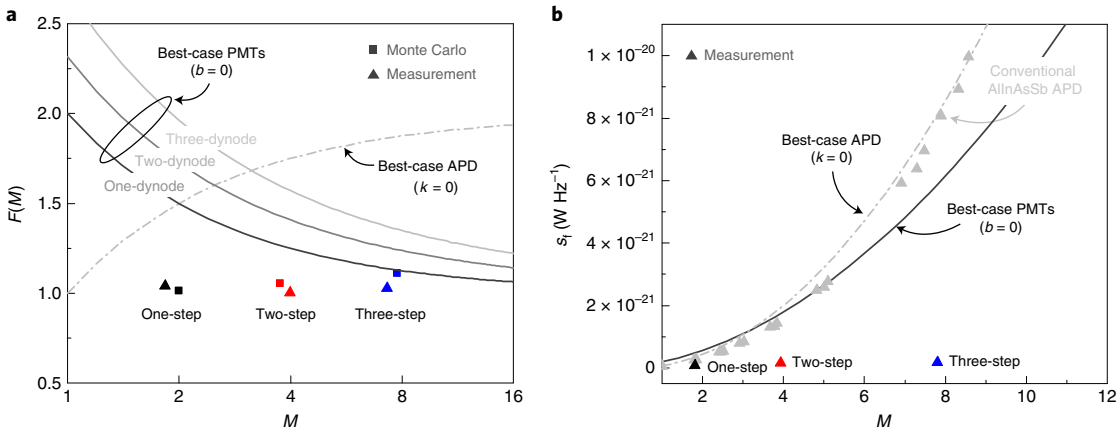

Fig. 5 | Measured and modelled staircase APD noise benefit at 300 K. a, Measured and simulated $F(M)$ for one-, two- and three-step staircase APDs indicate that low and approximately constant $F(M)$ near unity is expected. Measured data was found from fit-to-measurement M and p values from Fig. 4 and equation (1). Reference curves for the lowest expected noise for conventional APDs ($k=0$) and for the lowest noise one-, two- and three-dynode PMTs ($b=0$) show larger, less desirable $F(M)$ compared with multistep staircase APDs. **b**, Noise power spectral density versus gain in the shot-noise limit measured directly with a noise figure analyser for one-, two- and three-step staircase APDs. Also shown are reference curves for the best case conventional APDs and best case three-dynode PMT, along with measured values for a conventional $Al_xIn_{1-x}As_ySb_{1-y}$ digital alloy p–i–n APD that is known to exhibit $k\approx0$ low-noise behaviour at low gains[31]. The measured staircase data fall well below the best case detector curves, in excellent agreement with Monte Carlo calculations shown in Supplementary Fig. 8. The measured staircase noise power more closely follows a linear, rather than quadratic, dependence on gain.

resistance of the noise figure analyser (see the Methods for details). The second term $\sigma^2_{circuit}/\Delta f$ is the external circuit noise power spectral density, where Δf is the measurement bandwidth. Figure 5b plots noise power spectral density against gain of both $k=0$ APDs and $b=0$ PMTs, for the case when the circuit noise is smaller than the detector noise and the detector is shot-noise limited. Both exhibit the classic quadratic dependence of noise power with the gain, as do measurements of a $k\approx0$ AlInAsSb p–i–n APD included for completeness. Also shown in Fig. 5b are measured noise powers for the one-, two- and three-step staircase APDs.

Remarkably, our measurements show that the staircase noise power increases considerably more slowly than for either conventional APDs or PMTs. Figure 5b predicts that the three-step staircase APD should exhibit ~50-fold lower noise power than conventional $k=0$ APDs and ~30-fold lower noise power than $b=0$ PMTs at the same gain. Moreover, the measured noise power more closely follows a linear, rather than quadratic, dependence upon gain; this is consistent with Monte Carlo noise power simulations described in the Methods and Supplementary Fig. 8. This anomalously low noise power was unexpected and is likely a unique consequence of the single-carrier initiated, discrete localization of impact ionization events inherent to the staircase architecture. This holds tremendous promise for greatly increasing device signal-to-noise ratio (SNR) beyond the limits of existing detector technologies, which inherently exhibit the quadratic noise power dependence upon gain seen in equation (2). This is illustrated in Fig. 6, which plots the ratio between the signal-to-shot-noise ratios for the staircase APDs and conventional APDs versus multiplication. The ratio grows approximately linearly with M, regardless of k for the conventional APD.

Discussion

We have demonstrated that AlInAsSb staircase APDs with electron-initiated, discretely localized impact ionization events produce near-unity p values, resulting in deterministic 2^N gain scaling with N and extremely low noise. Furthermore, staircase APD behaviour indicates fundamentally improved noise characteristics over conventional APDs, and this added noise benefit is expected to scale favourably with gain as step count increases.

The primary challenge to further step scaling is the finite background carrier concentration in unintentionally doped AlInAsSb and the impact it has on band curvature. There is room for optimism in this regard as one of the AlInAsSb digital alloy binary constituents, InAs, has shown approximately two-orders-of-magnitude-lower background carrier concentration under optimized growth conditions[42,43]. Furthermore, we have recently realized AlInAsSb with background carrier concentrations of ~1×10^{15} cm^{-3} (around ten-fold lower than those in this study) through refinements in the growth process. Corrective techniques, such as compensation or delta-doping[25,44] to favourably adjust the electric field profile, could also be employed in the future to yield wider 2^N operating bias ranges. The other key challenge is to reduce the dark current; fortunately, the band-engineering flexibility of AlInAsSb affords considerable opportunities to reduce dark currents by suppressing band-to-band tunnelling across each step. We have recently demonstrated that the dark currents of one-step staircase APDs could be reduced by ~100-fold with only a minimal impact on gain.

The staircase APD clearly mimics the discrete gain performance associated with PMTs, consistent with its original conception as the solid-state analogue of the PMT[22,23]. Unlike PMTs, however, staircase APDs exhibit a weaker dependence of normalized noise power on gain. This advantage over PMTs has its primary origin in the stochasticity of the Poissonian dynode secondary electron yield, μ, which is known to vary between one and four secondary electrons produced per dynode generation event[1,14,15]. Further sources of PMT gain noise include variations in the primary electron velocities and spatial non-uniformity of the electric field between dynodes, which result in a spread in the electron trajectories and carrier transit times within PMTs[15,20]. By contrast, the staircase APD operates with a tighter, Bernoulli-like distribution of impact ionization yield at each step, greater uniformity of electric fields, and reduced susceptibility to geometrical constraints that cause carrier trajectory spread, resulting in fundamentally lower noise.

To put these results into context, as shown in Fig. 6, we considered the SNR ratios of the staircase APDs compared with conventional low-noise APDs. We used the linear normalized noise power relationship found in Fig. 5b and estimated a SNR improvement of 20 and 50 dB over conventional solid-state detectors for gains

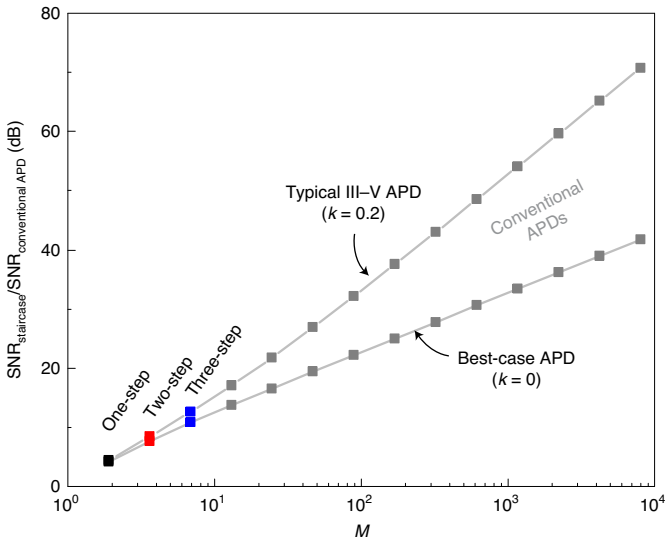

Fig. 6 | Estimated SNR comparison between staircase and conventional APDs in the shot-noise limit. Comparisons between the staircase APDs and a range of conventional APDs using a constant staircase of $F(M)=1.07$ and $p=0.9$ for the staircases. Typical APDs can operate with a gain between 100 and 1,000, and we predict that the SNR ratio would improve by 20 to 50 dB using the staircase APD over this range of gains.

between 100 and 1,000. Direct SNR comparison between staircase APDs and PMTs is difficult, but the linear versus quadratic noise power dependence suggests that staircase APDs probably experience a SNR benefit that grows approximately M-times faster than a PMT, which is substantial even for modest values of N. This effect is even more pronounced when staircase APDs are compared with more realistic PMTs ($0>b>1$) whose SNR grows as $\sim\mu^2/(\mu^2 b+\mu)$ and asymptotically approaches[1] $1/b$.

In the ideal case, the staircase steps cause high-energy electrons to only initiate a single impact ionization event. We do see evidence of spread in the carrier gain distribution with Monte Carlo analysis (Fig. 2e), suggesting deviation from the ideal case; however, it is well-known from Shockley et al.[45] and Friis[46] that the noise of the first stage of a multistage amplifier is the most important, with each successive stage wielding less influence on the overall noise. The carrier distribution models shown in Fig. 2e suggest that the first step is the least noisy with each successive step becoming noisier; this favourable arrangement should still produce low overall noise values at further elevated step counts.

As p approaches unity, $F(M)$ ceases to be a useful APD performance metric—there must be other, more dominant, sources of noise that should be considered, or a reformulation of the excess noise factor is required. For example, the APD noise power from equation (2) was derived for double-carrier, non-discrete impact ionization events across a uniform gain medium[18], which we see is not valid in Fig. 2b–d; this results in the anonymously low dependence of the noise power with multiplication shown in Fig. 5b. Comparing normalized noise power (Supplementary Fig. 8), the three-step staircase APD exhibited approximately tenfold lower normalized noise power than the best-case APDs and around threefold lower normalized noise power than the best-case PMTs with the same gain, which would directly translate into an approximately tenfold higher SNR compared with those ideal detectors—we report a lower noise detector than a PMT, which has been the most sensitive room-temperature-amplified detector throughout its >70-year history, but with the benefits afforded by a solid-state platform.

The Monte Carlo simulations presented were produced from conventional first-principles expressions for carrier transport and agree well with measurements, suggesting that there is no need to introduce new physics to capture the deterministic, low-noise behaviour of the staircase APD. However, the deviation from the classic quadratic noise power theory reinforces the need to develop a better noise model for this new class of extremely low-noise APD.

Conclusion

We report the first demonstration of staircase APDs that operate as anticipated with gain scaling as 2^N, confirmed with measurements and Monte Carlo simulations. Importantly, we have also identified unexpectedly low-noise properties that stem from the inherent determinicity of impact ionization at each step. As a result, this becomes a room-temperature-amplified detector that could eventually prove more sensitive than PMTs, but with the advantages afforded by a solid-state platform, including the potential for two-dimensional imaging arrays and wavelength flexibility by adjusting the absorber bandgap[33,34]. Future work will focus on scaling to still higher step counts, hence higher gains; however, the estimated SNR ratios presented in Fig. 6 suggest that staircase APDs with only a few steps can already compete directly with conventional APDs and find rapid deployment. Ultralow noise impact-ionization-engineered (I^2E) APDs already find application in position sensing and communications[47] despite only offering low noise up to gains on the order of ten, similar to the gain levels demonstrated here experimentally.

Online content

Any methods, additional references, Nature Research reporting summaries, source data, extended data, supplementary information, acknowledgements, peer review information; details of author contributions and competing interests; and statements of data and code availability are available at https://doi.org/10.1038/s41566-021-00814-x.

Received: 5 May 2020; Accepted: 8 April 2021;
Published online: 20 May 2021

References

1. Engstrom, R. W. et al. *Photomultiplier Manual* (RCA Corporation, 1970).
2. Iams, H. & Salzberg, B. The secondary emission phototube. *Proc. IRE* **23**, 55–64 (1935).
3. Morton, G. A. Photomultipliers for scintillation counting. *RCA Rev.* **10**, 525–553 (1949).
4. Hadfield, R. H. Single-photon detectors for optical quantum information applications. *Nat. Photon.* **3**, 696–705 (2009).
5. Yalow, R. S. & Berson, S. A. Assay of plasma insulin in human subjects by immunological methods. *Nature* **184**, 1648–1649 (1959).
6. Phelps, M. E., Hoffman, E. J., Mullani, N. A. & Ter-Pogossian, M. M. Application of annihilation coincidence detection to transaxial reconstruction tomography. *J. Nucl. Med.* **16**, 210–224 (1975).
7. The ATLAS Collaboration. The ATLAS experiment at the CERN Large Hadron Collider. *J. Instrum.* **3**, S08003 (2008).
8. Suzuki, Y. & Satellite, K. The super-Kamiokande experiment. *Eur. Phys. J. C* **79**, 298 (2019).
9. Giacconi, R., Gursky, H., Paolini, F. R. & Rossi, B. B. Evidence for X-rays from sources outside the solar system. *Phys. Rev. Lett.* **9**, 439–443 (1962).
10. Zworykin, V. A., Hillier, J. & Snyder, R. L. A scanning electron microscope. *Bull. Am. Soc. Test. Mater.* **117**, 15–23 (1942).
11. Hell, S. W. & Wichmann, J. Breaking the diffraction resolution limit by stimulated emission: stimulated-emission-depletion fluorescence microscopy. *Opt. Lett.* **19**, 780 (1994).
12. König, K. Clinical multiphoton tomography. *J. Biophoton.* **1**, 13–23 (2008).
13. *Photomultiplier Tubes: Photomultiplier Tubes and Related Products* (Hamamatsu Photonics, 2016).
14. Bay, Z. & Papp, G. Determination of the probability distribution of the number of secondary electrons. *IEEE Trans. Nucl. Sci.* **11**, 160–168 (1964).
15. Prescott, J. R. A statistical model for photomultiplier single-electron statistics. *Nucl. Instrum. Methods* **39**, 173–179 (1966).
16. Lachs, G. The statistics for the detection of light by nonideal photomultipliers. *IEEE J. Quantum Electron.* **10**, 590–596 (1974).

17. Campbell, J. C. et al. Recent advances in avalanche photodiodes. *IEEE J. Sel. Top. Quantum Electron.* **10**, 777–787 (2004).
18. McIntrye, R. J. Multiplication noise in uniform avalanche diodes. *IEEE Trans. Electron Devices* **13**, 164–168 (1966).
19. Matsuo, K., Teich, M. C. & Saleh, B. E. A. Noise properties and time response of the staircase avalanche photodiode. *IEEE Trans. Electron Devices* **32**, 2615–2623 (1985).
20. Teich, M. C., Matsuo, K. & Saleh, B. E. A. Excess noise factors for conventional and superlattice avalanche photodiodes and photomultiplier tubes. *IEEE J. Quantum Electron.* **22**, 1184–1193 (1986).
21. Chin, R., Holonyak, N., Stillman, G. E., Tang, J. Y. & Hess, K. Impact ionisation in multilayered hetero junction structures. *Electron. Lett.* **16**, 467–469 (1980).
22. Williams, G. F., Capasso, F. & Tsang, W. T. The graded bandgap multilayer avalanche photodiode: a new low-noise detector. *IEEE Electron Device Lett.* **3**, 71–73 (1982).
23. Capasso, F., Tsang, W. T. & Williams, G. F. Staircase solid-state photomultipliers and avalanche photodiodes with enhanced ionization rates ratio. *IEEE Trans. Electron Devices* **30**, 381–390 (1983).
24. Ripamonti, G. et al. Realization of a staircase photodiode: towards a solid-state photomultiplier. *Nucl. Instrum. Methods Phys. Res. A* **288**, 99–103 (1990).
25. Toivonen, M., Salokatve, A., Hovinen, M. & Pessa, M. GaAs/AIGaAs delta-doped staircase avalanche photodiode with separated absorption layer. *Electron. Lett.* **28**, 32–34 (1992).
26. Czajkowski, I. K., Allam, J. & Adams, A. R. Role of satellite valleys in ionisation rate enhancement in multiple quantum well avalanche photodiodes. *Electron. Lett.* **26**, 1311–1313 (1990).
27. Tsuji, M., Watanabe, I., Makita, K. & Taguchi, K. InAlGaAs staircase avalanche photodiodes. *Jpn. J. Appl. Phys.* **33**, L32–L34 (1994).
28. Lambert, B. et al. Feasibility of 1.5 µm staircase solid state photomultipliers in the AlGaSb/GaInAsSb system. *Semicond. Sci. Technol.* **11**, 226 (1996).
29. Vaughn, L. G., Dawson, L. R., Xu, H., Jiang, Y. & Lester, L. F. *Characterization of AlInAsSb and AlGaInAsSb MBE-grown Digital Alloys* Vol. 744, 397–408 (MRS Online Proceedings Archive, 2002).
30. Maddox, S. J., March, S. D. & Bank, S. R. Broadly tunable AlInAsSb digital alloys grown on GaSb. *Cryst. Growth Des.* **16**, 3582–3586 (2016).
31. Woodson, M. E. et al. Low-noise AlInAsSb avalanche photodiode. *Appl. Phys. Lett.* **108**, 081102 (2016).
32. Yi, X. et al. Extremely low excess noise and high sensitivity $AlAs_{0.56}Sb_{0.44}$ avalanche photodiodes. *Nat. Photon.* **13**, 683–686 (2019).
33. Ren, M. et al. AlInAsSb separate absorption, charge, and multiplication avalanche photodiodes. *Appl. Phys. Lett.* **108**, 191108 (2016).
34. Jones, A. H., March, S. D., Bank, S. R. & Campbell, J. C. Low-noise high-temperature AlInAsSb/GaSb avalanche photodiodes for 2-µm applications. *Nat. Photon.* **14**, 559–563 (2020).
35. Zheng, J. et al. Characterization of band offsets in $Al_xIn_{1-x}As_ySb_{1-y}$ alloys with varying Al composition. *Appl. Phys. Lett.* **115**, 122105 (2019).
36. Bank, S. R. et al. Avalanche photodiodes based on the AlInAsSb materials system. *IEEE J. Sel. Top. Quantum Electron.* https://doi.org/10.1109/JSTQE.2017.2737880 (2018).
37. Ren, M. et al. AlInAsSb/GaSb staircase avalanche photodiode. *Appl. Phys. Lett.* **108**, 081101 (2016).
38. David, J. P. R. Photodetectors: the staircase photodiode. *Nat. Photon.* **10**, 364–366 (2016).
39. Maddox, S. J. et al. Low-noise high-gain tunneling staircase photodetector. In *2016 74th Annual Device Research Conference* (IEEE, 2016).
40. Bude, J. & Hess, K. Thresholds of impact ionization in semiconductors. *J. Appl. Phys.* **72**, 3554–3561 (1992).
41. van der Ziel, A., Yu, Y. J., Bosman, G. & van Vliet, C. M. Two simple proofs of Capasso's excess noise factor FN of an ideal N-stage staircase multiplier. *IEEE Trans. Electron Devices* **33**, 1816–1817 (1986).
42. Maddox, S. J. et al. Enhanced low-noise gain from InAs avalanche photodiodes with reduced dark current and background doping. *Appl. Phys. Lett.* **101**, 151124 (2012).
43. Sun, W. et al. High-gain InAs avalanche photodiodes. *IEEE J. Quantum Electron.* **49**, 154–161 (2013).
44. Pilotto, A. et al. Optimization of GaAs/AlGaAs staircase avalanche photodiodes accounting for both electron and hole impact ionization. *Solid State Electron.* **168**, 107728 (2020).
45. Shockley, W. & Pierce, J. R. A theory of noise for electron multipliers. *Proc. IRE* **26**, 321–332 (1938).
46. Friis, H. T. Noise figures of radio receivers. *Proc. IRE* **32**, 419–422 (1944).
47. Ferraro, M. S. et al. Position sensing and high bandwidth data communication using impact ionization engineered APD arrays. *IEEE Photon. Technol. Lett.* **31**, 58–61 (2019).
48. Forrest, S. R. Performance of $In_xGa_{1-x}As_yP_{1-y}$ photodiodes with dark current limited by diffusion, generation recombination, and tunneling. *IEEE J. Quantum Electron.* **17**, 217–226 (1981).

Methods

Epitaxial growth. Device structures were grown on n-type GaSb(001) substrates at a growth temperature of 450–480 °C, as determined by blackbody thermometry (k-Space BandiT). Solid-source valved-crackers provided As_2 and Sb fluxes, and solid-source effusion cells provided Al, Ga, In, Be (acceptor) and GaTe (donor) fluxes. The AlInAsSb layers were grown as digital alloys of stable binaries using the repeating layer sequence: AlSb, AlAs, AlSb, InSb, InAs, Sb (5 s soak) with a total period thickness of ten monolayers (ML). The relative layer thicknesses were adjusted as-required to perform compositional grading. The following v:III beam equivalent pressure ratios were used: Sb:Al ≈ 20, Sb:In ≈ 7, As_2:Al ≈ 14, As_2:In ≈ 5. AlInAsSb compositions were strain-balanced to GaSb(001) using high-resolution X-ray diffraction and grown at 0.75 ML s^{-1} to produce well-defined superlattice interfaces. Sample rotation was 22.5 r.p.m. to synchronize with the growth rate and shutter timings to assure layer uniformity. Further growth details and properties of the resulting materials are reported elsewhere[29,30,35].

Device fabrication. Circular mesas with 100 µm diameters were defined by standard photolithography processes and chemically etched using a phosphoric/citric acid solution. Titanium/gold p- and n-type Ohmic contacts were deposited by electron-beam evaporation and the mesa sidewalls were passivated with SU-8 to further reduce surface leakage. An example fabrication process flow is shown in Supplementary Fig. 1 and representative scanning electron microscope images of the fabricated devices are shown in Supplementary Fig. 2.

Current–voltage characteristics. Current–voltage (I–V) characteristics were measured with a Keithley 2400 source meter under blackout (dark) and illuminated (light) conditions at room temperature, as shown in Supplementary Fig. 3. A 543 nm He–Ne continuous-wave laser was used to illuminate the APDs with ~0.1 mW of power focused onto the top of the sample surface, which resulted in >99.9% absorption of the incident radiation in the p-contact layer and above-the-step UID region. The photocurrent was calculated as the difference between light and dark I–V curves. Temperature-dependent measurements were performed in a liquid-nitrogen-cooled cryogenic chamber and measured with a Agilent 4155 semiconductor parameter analyser.

Multiplication gain. We followed the same gain calculation method established in ref. [37] and determined the multiplication gain by normalizing each staircase APD photoresponse to their corresponding p–i–n control structure. We calculated the photocurrent (I_{photo}) from the total illuminated current (I_{total}) and dark current (I_{dark}) for both the staircase APD and its step-free control as: $I_{photo} = I_{total} - I_{dark}$. Next, the photogain M shown in Fig. 3 was calculated as follows: $M = I_{photo,staircase}/I_{photo,control}$. Normalizing directly to a homojunction p–i–n control allowed us to directly measure the multiplication gain caused by the presence of the staircase step(s). Over the measured and simulated (see the next section) bias range in which the staircase demonstrated 2^N gain, the p–i–n control structures exhibited a flat photoresponse versus bias (see Supplementary Fig. 3), indicating that neither conventional impact ionization gain nor band-to-band tunnelling breakdown occurred before staircase breakdown. Supplementary Fig. 4 describes the measured gain algorithm and staircase operating range. The presence of tunnelling breakdown was corroborated using temperature-dependent dark current density measurements (see Supplementary Fig. 5).

Capacitance–voltage characteristics. Capacitance–voltage characteristics in Supplementary Fig. 6 were measured under blackout conditions with a calibrated HP 4275 A LCR meter at 1 MHz.

Monte Carlo simulations. Transport expressions for semiconductor carrier scattering mechanisms were derived from first-principles using Fermi's golden rule and impact ionization was modelled using the Keldysh formula[49,50]. Material parameters used to model AlInAsSb were determined from homojunction p–i–n APDs and are reported elsewhere[33,51].

To achieve appropriate gain distribution statistics, 10,000 simulation iterations were run for each device in 1 V bias increments, where Poisson's equation was self-consistently solved at each bias step. Noise power performance of both staircase devices and their p–i–n controls were evaluated using time-dependent, first-principles expressions[52] (see Supplementary Fig. 7 for an example) to compute s_f versus frequency, f, within the shot-noise limit, using:

$$s_f = 2\langle n \rangle \, |I(f)|^2$$

where $\langle n \rangle$ is the average number of charge carriers produced from a simulation run and $I(f)$ is the Fourier transform of the time-dependent current, $I(t)$, which was calculated from Ramo's Theorem using the junction's depletion region thickness, L, and individual carrier velocity, $v_i(t)$:

$$I(t) = \frac{q}{L} \sum_i v_i(t)$$

Noise power. Staircase APDs and a conventional AlInAsSb digital alloy p–i–n APD in Fig. 5b were biased at room temperature with a Keithley 2400 source meter. A 543 nm He–Ne continuous-wave laser was used to illuminate the APDs. The alternating current component of the output current was measured with an Agilent 8,973 A noise figure analyser with a 50 Ω load impedance through a standard radio frequency bias tee. Careful system calibration was carried out via a calibrated Agilent 346 A noise source to remove background noise. Devices were measured and simulated in the 2^N gain regime over a 4 MHz bandwidth centred at 50 MHz. In Fig. 5b, the noise power spectral density data points were scaled according to their measured unity-gain photocurrents to allow for an accurate comparison. Supplementary Fig. 8 describes the normalized noise power, which was computed by dividing each staircase noise power value by the noise power for its corresponding control p–i–n (which we define as $\langle M \rangle = 1$). Conventional APD and PMT detector reference curves shown in Supplementary Fig. 8 were calculated using equation (2) and (S1).

SNR estimation. We assumed reasonable performance values for the staircase[37] and conventional low-noise APDs[17], using external quantum efficiencies of 80%, photocurrents of 10 µA, and dark currents of 1 µA. In the shot-noise limit, the ratio of $SNR_{staircase}$ to $SNR_{conventional\ APD}$ as a function of gain can be approximated from equation (2) as:

$$\frac{SNR_{staircase}}{SNR_{conventional\ APD}} \approx M \left(\frac{F(M)_{conventional\ APD}}{F(M)_{staircase}} \right)$$

where a $F(M)_{staircase}$ value of 1.07 was found from Fig. 5b and $F(M)_{conventional\ APD} = kM + (1-k)\left(2 - \frac{1}{M}\right)$; k is the ratio of the electron to hole impact ionization coefficients and the average gain is $\langle M \rangle = (1+p)^N$ assuming a fixed value of $p = 0.9$ (see Fig. 4a).

Data availability

The data that support the plots within this paper and other findings of this study are available from the corresponding author on reasonable request. Source data are provided with this paper.

Code availability

Simulation software used to produce electrostatic models are available at the following GitHub repository: https://github.com/scott-maddox/openbandparams.

References

49. Hess, K. *Advanced Theory of Semiconductor Devices* (Wiley, 2000).
50. Ma, F. et al. Monte Carlo simulations of $Hg_{0.7}Cd_{0.3}Te$ avalanche photodiodes and resonance phenomenon in the multiplication noise. *Appl. Phys. Lett.* **83**, 785–787 (2003).
51. Yuan, Y. et al. AlInAsSb impact ionization coefficients. *IEEE Photon. Technol. Lett.* **31**, 315–318 (2019).
52. van der Ziel, A. *Noise in Solid State Devices and Circuits* (John Wiley & Sons, 1986).

Acknowledgements

This work was supported by the Army Research Office and DARPA (contract no. W911NF-17-1-0065) and DARPA (contract no. W909MY-12-D-0008). We acknowledge use of Texas Nanofabrication Facilities supported by the NSF NNCI Award 1542159.

Author contributions

S.D.M. and S.R.B. carried out simulations, crystal growth and materials characterization. A.H.J. and J.C.C. were responsible for device fabrication and experimental characterization. Analysis was performed by S.D.M. and A.H.J. S.D.M. and A.H.J. wrote the paper with assistance from J.C.C. and S.R.B. S.D.M., A.H.J., J.C.C. and SRB all contributed to the structure design.

Competing interests

The authors declare no competing interests.

Additional information

Supplementary information The online version contains supplementary material available at https://doi.org/10.1038/s41566-021-00814-x.

Correspondence and requests for materials should be addressed to S.D.M. or S.R.B.

Peer review information *Nature Photonics* thanks M. Saif Islam and the other, anonymous, reviewer(s) for their contribution to the peer review of this work.

Reprints and permissions information is available at www.nature.com/reprints.